

# Building patterns by traveling vortices and dipoles in periodic dissipative media

Valentin Besse<sup>1</sup>, Hervé Leblond<sup>1</sup>, Dumitru Mihalache<sup>1,2,3</sup> and Boris A. Malomed<sup>4</sup>

<sup>1</sup> *LUNAM Université, Université d'Angers, Laboratoire de Photonique d'Angers, EA 4464, 2 Boulevard Lavoisier, 49000 Angers, France*

<sup>2</sup> *Horia Hulubei National Institute for Physics and Nuclear Engineering, 30 Reactorului, Magurele-Bucharest, 077125, Romania*

<sup>3</sup> *Academy of Romanian Scientists, 54 Splaiul Independentei, 050094 Bucharest, Romania*

<sup>4</sup> *Department of Physical Electronics, Faculty of Engineering, Tel Aviv University, Tel Aviv 69978, Israel*

We analyze pattern-formation scenarios in the two-dimensional (2D) complex Ginzburg-Landau (CGL) equation with the cubic-quintic (CQ) nonlinearity and a cellular potential. The equation models laser cavities with built-in gratings, which are used to stabilize 2D patterns. The pattern-building process is initiated by kicking a localized compound mode, in the form of a dipole, quadrupole, or vortex which is composed of four local peaks. The hopping motion of the kicked mode through the cellular structure leads to the generation of various extended patterns pinned by the structure. In the ring-shaped system, the persisting freely moving dipole hits the stationary pattern from the opposite side, giving rise to several dynamical regimes, with the pinned multi-soliton chain playing the role of the Newton's cradle (NC).

PACS numbers: 47.54.-r, 47.20.Ky, 42.65.Tg, 42.65.Sf

## I. INTRODUCTION

The fundamental principle behind the creation of dissipative solitons is that their stability relies upon the simultaneous balance of conservative and dissipative ingredients in the underlying system [1]. These are the diffraction and self-focusing nonlinearity in the conservative part of the system, and linear and nonlinear loss and gain terms in the dissipative part. Well-known physical realizations of such systems are offered by lasing [2, 3] and plasmonic [4] cavities, the respective models being based on the complex Ginzburg-Landau (CGL) equations with the cubic-quintic (CQ) sets of gain and loss terms, combined with the background linear loss [3]. This combination is well known to maintain stable localized modes [5]. The CGL equations constitute a generic class of dissipative pattern-formation models [6], which find many other applications, including bosonic condensates of quasi-particles in solid-state media [7], reaction-diffusion systems [8], and superconductivity [9].

Originally, the CGL equation of the CQ type was introduced [5] as a model for the creation of stable two-dimensional (2D) localized modes. Following this work, similar models were derived or proposed as phenomenological ones in various settings. Many 1D and 2D localized states, i.e., dissipative solitons, have been found as solutions of such equations [10]-[15].

An essential ingredient of highly-functional laser cavities is a transverse periodic grating, which can be fabricated by means of available technologies [16]. In addition to the permanent gratings, virtual photonic lattices may be induced in photorefractive crystals as interference patterns by pairs of pump beams with the ordinary polarization, which illuminate the crystal along axes  $x$  and  $y$ , while the probe beam with the extraordinary polarization is launched along  $z$  [17]. A 2D cavity model with the grating was introduced in Ref. [18]. It is based on the CQ-CGL equation including the cellular (lattice) potential, which represents the grating. In fact, the laser cavity equipped with the grating may be considered as a photonic crystal built in the active medium. Periodic potentials also occur in models of passive optical systems, which are driven by external beams and operate in the temporal domain, unlike the active systems which act in the spatial domain [19, 20].

Localized vortices, alias vortex solitons, are an important species of self-trapped modes in 2D settings. In uniform media, dissipative vortex solitons cannot be stable without the presence of a diffusion term (see, e.g., Ref. [12]), which is, however, absent in models of waveguiding systems (this term may sometimes be relevant in temporal-domain optical models [21]). Nevertheless, compound vortices, built as complexes of four peaks pinned to the lattice potential, may be stable in models including the grating in the absence of the diffusion [18]. Using this possibility, stable 2D [22] and 3D [23] vortical solitons were studied in detail in the framework of CGL equations including trapping potentials.

In most previous works, the studies of various 2D localized patterns have been focused on their stabilization by means of the lattice potentials. Another interesting issue is mobility of 2D dissipative solitons in the presence of the underlying lattice (dissipative solitons may move freely only if the diffusion term is absent, therefore the mobility is a relevant issue for the diffusion-free models of laser cavities). Localized modes can be set in motion by the application of a kick to them, which, in the context of the laser-cavity models, implies launching a tilted beam into the system. Recently, the mobility of kicked 2D fundamental solitons in the CQ-CGL equation with the cellular potential was studied in Ref. [24]. It has been demonstrated that the kicked soliton, hopping through the periodic structure, leaves

in its wake various patterns in the form of finite multi-peak chains trapped by the periodic potential. In the case of periodic boundary conditions (b.c.), which correspond to an annular system, the free soliton completes the round trip and hits the chain that it has originally created. Depending on parameters, the collision of the free soliton with the pinned chain may proceed in the Newton-cradle (NC) regime, ending with the release of a free soliton from the opposite edge of the chain. Thus, the NC impact in the ring-shaped setup may repeat itself periodically, which is one of dynamical pattern-formation scenarios produced by the system. Another generic outcome of the evolution was “NC with absorption”, which implies that the free soliton was absorbed by the chain after several (up to five) collision cycles [24].

A natural extension of the analysis performed in Ref. [24] is the study of the mobility of kicked soliton complexes, such as dipoles, quadrupoles, and compound vortices, and various scenarios of the dynamical pattern formation by such moving complex modes, in the framework of the 2D CQ-CGL equation with the lattice potential. The model is formulated in Section II, which is followed by the presentation of systematic numerical results for dipoles, quadrupoles, and vortices of two types (“rhombuses” and “squares”, alias onsite and intersite-centered ones) in Sections III, IV, and V, respectively. The paper is concluded by Section VI.

In particular, an essential finding, which is reported in Section III, is that the pattern-formation processes, initiated by the motion of a kicked dipole, feature new realizations of the NC in the interaction of freely moving solitons with pinned soliton chains. In this connection, it is relevant to mention that, besides the above-mentioned example of the NC in the same model, which was initiated by the motion of the kicked fundamental soliton [24], soliton “cradles” were reported previously as “super-fluxons” in pinned arrays of regular fluxons in long Josephson junctions with a lattice of defects [25], in chains of repulsively interacting matter-wave solitons in a model of binary Bose-Einstein condensates [26]. Very recently, it was reported that splitting of higher-order ( $N$ -) solitons in nonlinear optical fibers, under the action of the third-order group-velocity dispersion, proceeds via creating NCs in chains of temporal solitons [27].

## II. THE CUBIC-QUINTIC COMPLEX GINZBURG-LANDAU MODEL WITH THE CELLULAR POTENTIAL

The CQ-CGL equation with a periodic potential is written as

$$\frac{\partial u}{\partial Z} = \left[ -\delta + \frac{i}{2} \nabla_{\perp}^2 u + (i + \epsilon) |u|^2 u - (i\nu + \mu) |u|^4 + iV(X, Y) \right] u. \quad (1)$$

It describes the evolution of the amplitude of electromagnetic field  $u(X, Y, Z)$  along propagation direction  $Z$ , with transverse Laplacian  $\nabla_{\perp}^2 = \frac{\partial^2}{\partial X^2} + \frac{\partial^2}{\partial Y^2}$ . Parameter  $\delta$  is the linear-loss coefficient,  $\epsilon$  is the cubic gain,  $\mu$  the quintic loss, and  $\nu$  the quintic self-defocusing coefficient (it accounts for the saturation of the Kerr effect if  $\nu > 0$ ). The 2D periodic potential with amplitude  $V_0$  is taken in the usual form,  $V(X, Y) = V_0 [\cos(2X) + \cos(2Y)]$ , with the period normalized to be  $\pi$ . The total power of the field is also defined as usual,

$$P = \int \int |u(X, Y)|^2 dXdY. \quad (2)$$

We solved CGL equation (1) by means of the fourth-order Runge-Kutta algorithm in the  $Z$ -direction, and five-point finite-difference scheme for the computation of the transverse Laplacian  $\nabla_{\perp}^2$ . Periodic boundary conditions (b.c.) were used for the study of kicked dipoles, and absorbing b.c. for kicked vortices.

Values of coefficients chosen for numerical simulations are  $\delta = 0.4$ ,  $\epsilon = 1.85$ ,  $\mu = 1$ ,  $\nu = 0.1$ , and  $V_0 = -1$ . This choice corresponds to a set of parameters for which the initial static configuration is stable. We impart an initial velocity to it, adding the linear phase profile to the initial field of the static state:

$$u_0(X, Y) \rightarrow u_0(X, Y) \exp(i\mathbf{k}_0 \cdot \mathbf{r}), \quad (3)$$

where  $\mathbf{r} \equiv \{X, Y\}$ . The key parameters are length  $k_0$  of kick vector  $\mathbf{k}_0$ , and angle  $\theta$  which it makes with the  $X$ -axis, i.e.,

$$\mathbf{k}_0 = (k_0 \cos \theta, k_0 \sin \theta). \quad (4)$$

In the laser setup the kick corresponds to a small deviation of the propagation direction of the beam from the  $Z$  axis. If  $K_0$  is the full wave number and  $\varphi$  is the deviation angle, the length of the transverse wave vector in physical units is  $K_0 \sin \varphi$ , which corresponds to  $k_0$  in the normalized form. The aim of this work to investigate the influence of kick parameters  $k_0$  and  $\theta$ , defined as per Eq. (4), on a variety of multi-soliton complexes, which are created by moving dipoles, quadrupoles, or vortices (of both rhombus- and square-types) in the 2D CGL medium with the cellular potential.

### III. THE PATTERN FORMATION BY KICKED DIPOLES

#### A. Generation of multi-dipole patterns by a dipole moving in the transverse direction

In this Section we consider the simplest soliton complex in the form of a stable vertical dipole, which consists of a pair of solitons aligned along the  $Y$ -axis and mutually locked with phase difference  $\pi$ , which is shown in Fig. 1. First, the dipole is set in motion by the application of the kick in the horizontal ( $X$ ) direction (i.e., transversely, with respect to the dipole's axis), as per Eqs. (3) and (4) with  $\theta = 0$ . As shown in Fig. 2, the moving dipole multiplies itself into a set of secondary ones, similar to the outcome of the evolution of the kicked fundamental soliton [24]. Each newly created dipole features the fixed phase shift  $\pi$  between two constituent solitons, and the entire pattern, established as the result of the evolution, is quite robust.

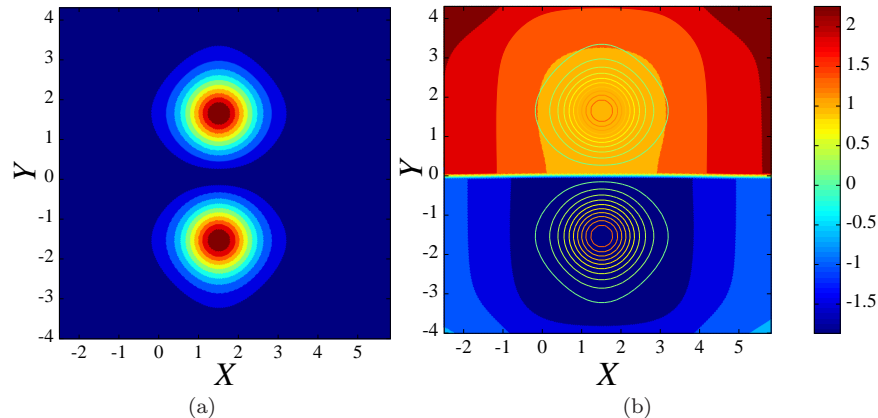


FIG. 1: (Color online) The distribution of the amplitude (a) and phase (in units of  $\pi$ ) (b) in the stable quiescent dipole mode.

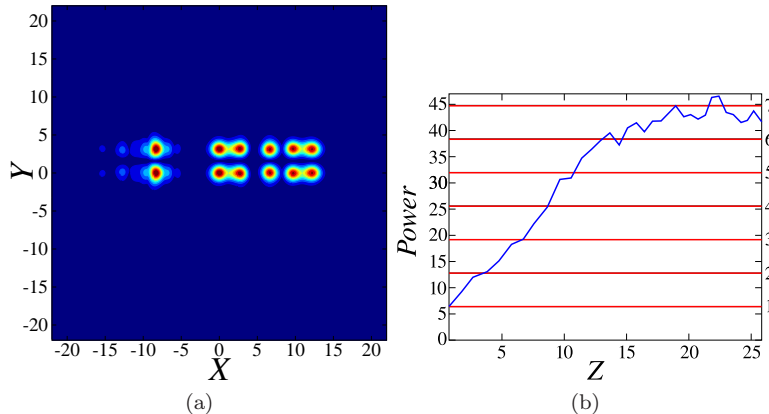


FIG. 2: (Color online) (a) Field  $|u(X, Y)|$  produced by the horizontally kicked (with  $\theta = 0$ ) vertical dipole at  $Z = 22.410$ , for  $k_0 = 1.665$ . In this panel, the leftmost dipole is moving to the right. (b) The evolution of the kicked dipole, shown in terms of the total power of the field as a function of propagation distance  $Z$ . The set of horizontal red lines show power levels corresponding to different numbers ( $n$ ) of quiescent dipoles.

The configuration displayed in Fig. 2 consists of a chain of five trapped dipoles, and a free one, which has wrapped up the motion and reappears from the left edge, moving to the right, due to the periodic b.c. Then, the free soliton is going to collide with the pinned chain, which may give rise to the NC dynamics, which is considered separately below.

The snapshot shown in Fig. 2 corroborates an inference made from the analysis of numerical results: The largest number of the dipoles generated by the initially kicked one is six, including one moving dipole and five identical quiescent modes. It is worthy to note that, as seen in Fig. 2(b), in this case the total power (2) of the finally established set of six dipoles is close to the net power corresponding to *seven* quiescent ones, which is explained by the observation that the power of the stable moving dipole is, approximately, twice that of its quiescent counterpart.

To study the outcome of this dynamical pattern-formation scenario in a systematic form, we monitored the number of output solitons as a function of  $k_0$ . The numerical results are summarized in Fig. 3.

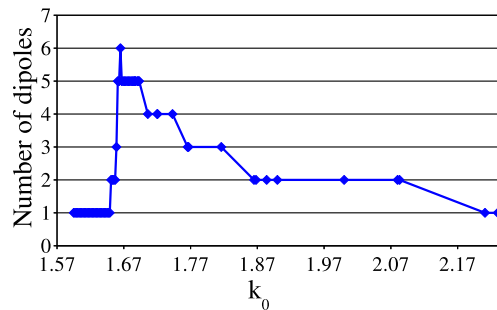


FIG. 3: (Color online) The number of dipoles in the final configuration versus the kick strength,  $k_0$ , applied to the original dipole in the horizontal direction.

Below the threshold value of the kick's strength, whose numerically found value is

$$k_0^{(\text{thr})}(\theta = 0) \approx 1.651, \quad (5)$$

the kicked dipole exhibits damped oscillations, remaining trapped near a local minimum of the cellular potential. Then, as seen in Fig. 3, the number of dipoles initially increases steeply with  $k_0$ , reaching (as mentioned above) a maximum of six at  $k_0 = 1.665$ . It is worthy to mention that this value is clearly different from those, ranging in interval  $k_0 \in [1.6927, 1.6942]$ , in which the maximum number of secondary solitons is reached in the case when the kick is applied to a fundamental soliton [24]. This observation suggests that building the structures by the kicked dipole does not merely reduce to the earlier studied regime of the pattern formation by the individual solitons forming the dipole. With the further increase of  $k_0$ , the number of solitons in the output decreases by increasingly broad steps.

### B. Dynamical regimes initiated by the longitudinal kick applied to the dipole

We have also simulated dynamical regimes initiated by the motion of the dipole kicked at angle of  $\theta = \pi/2$ , i.e., along its axis, see Eq. (4), which implies the possibility to generate not only new dipoles but fundamental solitons as well. It was found that the minimum value of the kick which is necessary to set the dipole in motion is smaller in this case than the one given by Eq. (5):

$$k_0^{(\text{thr})}(\theta = \pi/2) \approx 1.303. \quad (6)$$

The results obtained for this setting are summarized in Table I. Above the threshold value (6), additional moving solitons are created: one at  $k_0 \in [1.304, 1.875]$  and two in a narrow interval  $k_0 \in [1.880, 1.885]$ . Then, for  $k_0 \in [1.89, 2.015]$ , a new moving dipole appears, which, as well as the original one, is oriented along the direction of the motion, which is accompanied by two moving solitons. For  $k_0 \in [2.02, 2.17]$ , we have one moving soliton less, and at  $k_0 \in [2.175, 2.255]$  the original dipole disappears in the course of the propagation, thus leaving one moving dipole and two moving solitons in the system. At  $k_0 \in [2.26, 2.36]$ , we observe the same pattern as for  $k_0 \in [2.02, 2.17]$  (two dipoles and one moving soliton). Then, for  $k_0 \in [2.365, 2.46]$ , the dipole splits into two traveling solitons, with the upper one leaving a pinned soliton at the site which it originally occupied. At higher values of the kick's strength, the same pattern appears, except that the solitons do not leave anything behind them, just traveling through the lattice.

### C. Collision scenarios (Newton's cradle) for moving dipoles in the system with periodic b.c.

The above consideration was performed for a long system, before the collision of the freely moving dipole with the static pattern left in its wake, which should take place in the case of periodic b.c. In the application to laser-cavity settings, the periodic b.c. in the direction of  $X$  is relevant, corresponding to the cavity with the annular shape of its cross section. The study of dynamical pattern-formation scenarios with periodic b.c. is also interesting in its own right, in terms of the general analysis of models based on the CGL equations [24].

Behavior pattern	Range of $k_0$	Number of new solitons along $Y$ -direction
1 dipole	$k_0 \in [0, 1.303]$	0
1 dipole and 1 moving soliton	$k_0 \in [1.304, 1.875]$	1
1 dipole and 2 moving solitons	$k_0 \in [1.88, 1.885]$	2
2 dipoles and 2 moving solitons	$k_0 \in [1.89, 2.015]$	4
2 dipoles and 1 moving soliton	$k_0 \in [2.02, 2.17]$	3
1 dipole and 2 moving solitons	$k_0 \in [2.175, 2.255]$	2
2 dipoles and 1 moving soliton	$k_0 \in [2.26, 2.36]$	3
1 pinned and 2 moving solitons	$k_0 \in [2.365, 2.46]$	2
2 moving solitons	$k_0 \in [2.465, \infty)$	0

TABLE I: The number of dipoles and fundamental solitons in the established pattern versus the kick's strength  $k_0$  directed along the dipole's axis ( $\theta = \pi/2$ ). In the right column, a newly emerging dipole (if any) is counted as two solitons.

Under the periodic b.c., the freely moving dipole observed in Fig. 2 will complete the round trip and will hit the trapped chain of quiescent dipoles. Results of extensive simulations of this setting are summarized in the list of three different outcomes of the collisions, which feature persistent or transient dynamics of the NC type (all the regimes were observed for  $\theta = 0$ , i.e., the transversely kicked dipole):

- The NC regime proper, corresponding to periodically repeating effectively elastic collisions of the moving dipole with the finite chain of the quiescent ones, see Fig. 4. It take place for  $k_0 \in [1.865, 1.868]$  with  $\theta = 0$
- The “NC with absorption”, corresponding to several quasi-elastic collisions before the moving dipole is eventually absorbed by the quiescent chain, see Fig. 5. This transient regime occurs around  $k_0 = 1.816$  with  $\theta = 0$ .
- The “Transient NC with clearing the obstacle”, corresponding to several elastic collisions, before the stationary complex (the “cradle” itself) is absorbed by the moving dipole, see Fig. 6. This happens for  $k_0 \in [1.884, 1.9]$  and around  $k_0 = 2.083$  with  $\theta = 0$ .

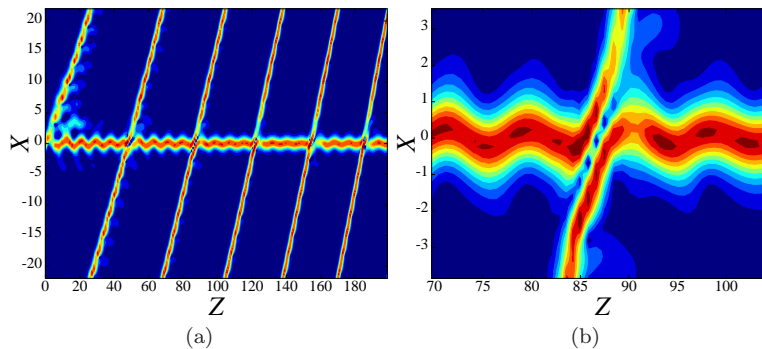


FIG. 4: (Color online) (a) The cross section of field  $|u(X, Y, Z)|$  at  $Y = 0$ , in the plane of  $(X, Z)$ , for  $k_0 = 1.865$ . This is an example of the NC scenario, when the moving dipole repeats elastic collisions with the finite chain of quiescent (trapped) ones. (b) The close-up of the NC interaction.

It is relevant to mention that the first two regimes have been reported in Ref. [24] for the motion of kicked fundamental solitons. However, the third regime is a new one, which was not found for the fundamental solitons. Another characteristic feature of this regime is that it eventually leads to the splitting of the surviving single dipole into unbound fundamental solitons, as shown in Fig. 7(a). To analyze the splitting, we have identified position  $\{X_c, Y_c\}$  of the field maximum in each soliton (its center), and values of phases at these points (mod  $2\pi$ ) as functions of evolution variable  $Z$ . As a result, it has been found that the splitting of the dipole and the loss of the phase correlation between its constituent solitons start in a “latent form” at  $Z \approx 102.8$ , and become explicit at  $Z \approx 112.5$ , see Figs. 7(c) and 7(d). The two solitons get completely separated at  $Z \approx 115$ . The splitting also leads to the appearance of the velocity difference between the solitons (the velocity is defined as  $dX_c/dZ$ ), as seen in Fig. 7(b).

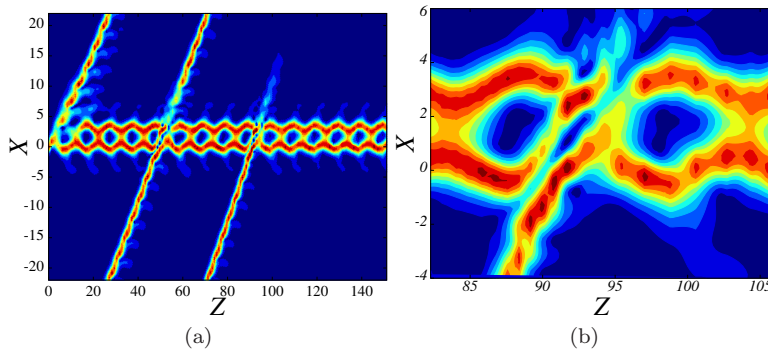


FIG. 5: (Color online) (a) The cross section of field  $|u(X, Y, Z)|$  at  $Y = 0$ , in the plane of  $(X, Z)$ , for  $k_0 = 1.816$ . This is an example of the “NC with absorption”, when the moving dipole is absorbed by the quiescent chain after several quasi-elastic collisions. (b) The close-up of the absorptive interaction.

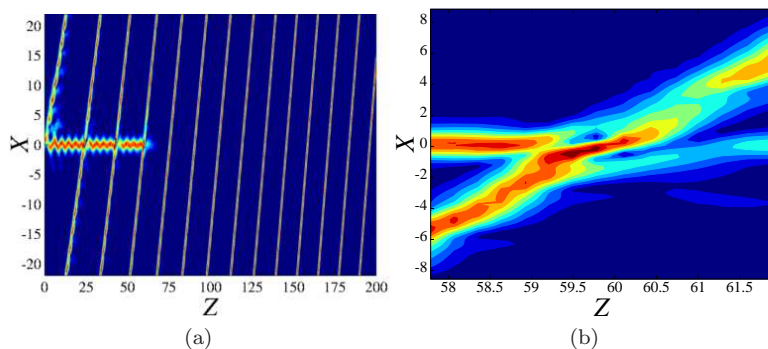


FIG. 6: (Color online) (a) The cross section of field  $|u(X, Y, Z)|$  at  $Y = 0$ , in the plane of  $(X, Z)$ , for  $k_0 = 1.884$ . This is an example of the “transient NC with clearing the obstacle”, when the moving dipole absorbs the stationary chain, after several collisions with it. (b) The close-up of the absorptive interaction.

#### IV. THE PATTERN FORMATION BY KICKED QUADRUPOLES

A quadrupole is composed of four soliton-like power peaks, which are mutually locked with a phase difference  $\pi$  between adjacent ones, see an example of the square-shaped (alias offsite-centered) quadrupole in Fig. 8. Although this mode carries no vorticity, simulations demonstrate that it is a very robust one. Similar to the previous section, we here aim to investigate dynamical regimes initiated by the application of the horizontal kick (3) to the quadrupole.

The quadrupole is set in motion by the kick whose strength exceeds the respective threshold,

$$k_0^{(\text{thr})}(\text{quadr}) = 1.28, \quad (7)$$

cf. Eqs. (5) and (6). The horizontal motion of the kicked quadrupole splits it into two vertical dipoles, and generates a set of additional vertically arranged quiescent *soliton pairs*, with a phase shift of  $\pi/2$  between them. The dependence of the total number of solitons in the eventually established pattern is shown, as a function of the kick strength  $k_0$ , in Fig. 9. The result is quite different from that reported in the previous section for the pattern formation by the kicked dipole, cf. Fig. 3.

Above the threshold value (7), the number of fundamental solitons in the emergent pattern increases and remains constant in a large interval of values of  $k_0$ , *viz.*, six solitons for  $k_0 \in [1.28, 1.865]$ . Then, the number of the solitons increases to its maximum, which is 16 at  $k_0 = 1.9$ . Note that the increase is not monotonous. For example, 12 solitons are generated at  $k_0 = 1.885$ , and then 10 solitons at  $k_0 = 1.887$ . Subsequently, in the interval of  $k_0 \in [1.91, 2.338]$ , the soliton number varies between 8 and 14. The largest number of solitons, 16, is reached again at  $k_0 \in [2.339, 2.341]$ . Then, the soliton number drops to 6, and this value remains constant over a relatively broad interval,  $k_0 \in [2.373, 2.475]$ . At still larger values of  $k_0$ , no additional solitons are generated by the initially moving quadrupole, which in this case again splits into two dipoles.



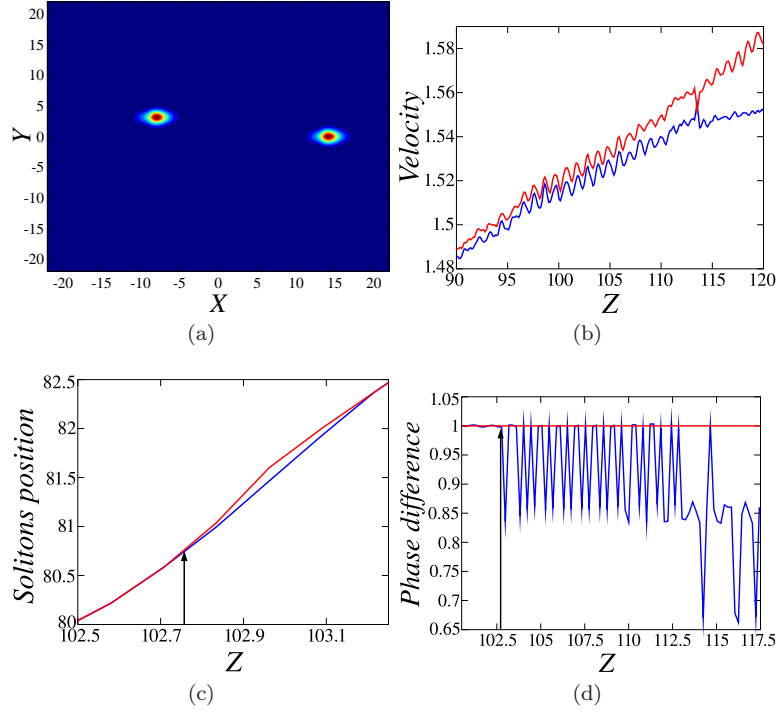


FIG. 7: (Color online) Illustration of the splitting of the single surviving dipole into uncorrelated fundamental solitons, which occurs in the “transient NC regime with clearing the obstacle”, after the absorption of the quiescent chain by the moving dipole, at  $k_0 = 1.884$ . (a) Field  $|u(X, Y)|$  at  $Z = 199.965$ . (b,c). Velocities and positions of both solitons as functions of  $Z$ . (d) The phase difference between the solitons versus  $Z$ , in units of  $\pi$ , the red horizontal line corresponding to the phase difference equal to  $\pi$ . The arrows in (c) and (d) indicate onset of the process eventually leading to the loss of the phase coherence and separation of the two solitons.

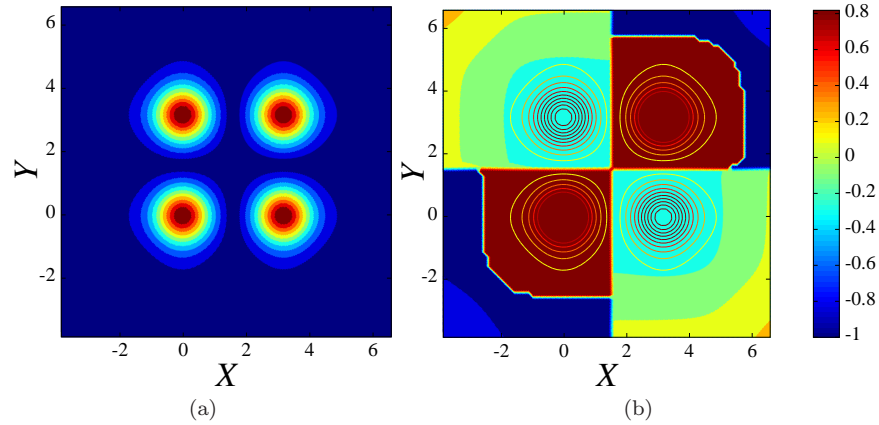


FIG. 8: (Color online) The distribution of the amplitude (a) and phase (in unites of  $\pi$ ) in the stable stationary square-shaped quadrupole used in the simulations.

At  $k_0 = 2.339$ , when the simulations generate the set of 16 solitons (the largest number, as said above), the set includes two moving dipoles, which are actually produced by the splitting of the original quadrupole, see Fig. 10(a). The faster dipole [whose trajectory is characterized by a larger slope (velocity),  $dX_c/dZ$ ] moves without creating new solitons, while the slower dipole creates several of them. Note that Fig. 10(a) shows only the constituent fundamental solitons on line  $Y = 0$ , in terms of Fig. 10(c), their counterparts on the line of  $Y = 3$  showing the same picture.

As mentioned above and shown in Fig. 11(a), at  $k_0 > 2.48$  the initial quadrupole splits into two dipoles, which move at different velocities, without the formation of additional soliton pairs. Figure 11(b) shows that each dipole remains locked with the phase difference of  $\pi$  between the constituent solitons (the jumps are due to a numerical

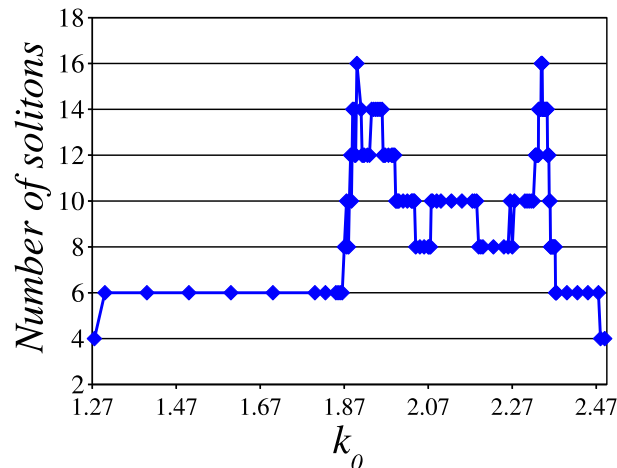


FIG. 9: (Color online) The total number of fundamental solitons in the pattern produced by kick  $k_0$  applied to the square-shaped quadrupole. Each dipole counts as two solitons.

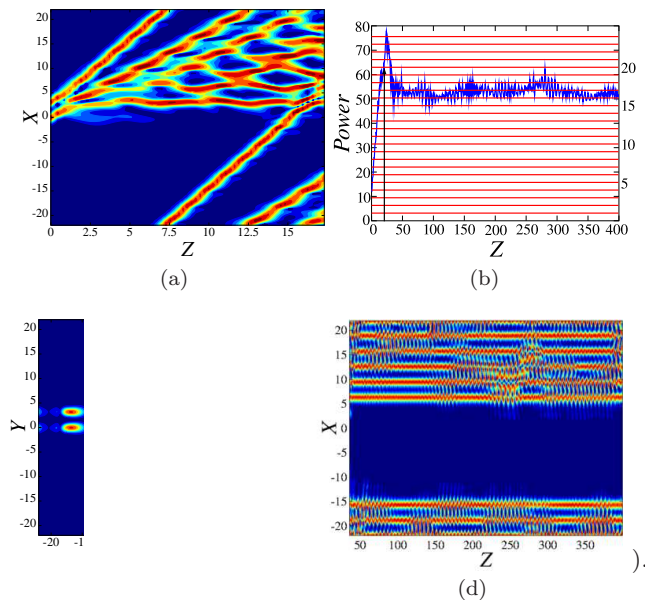


FIG. 10: (Color online) The evolution of the horizontally kicked quadrupole, for  $k_0 = 2.339$ . (a) Field  $|u(X, Y, Z)|$  in the cross section  $Y = 0$ , before the collision of the moving dipole with the pinned complex. (b) The total power versus  $Z$  (the arrow indicates the collision point); the horizontal red lines show the power corresponding to  $n$  quiescent fundamental solitons,  $n$  being the numbers indicated on the right vertical axis. (c) Field  $|u(X, Y)|$  at  $Z = 399.34$ . (d) Field  $|u(X, Y, Z)|$  in the cross section  $Y = 0$ , after the collision.

uncertainty).

## V. THE PATTERN FORMATION BY KICKED VORTICES

### A. Chaotic patterns generated by kicked rhombic (onsite-centered) vortices

It is well known that the lattice potential supports localized vortical modes of two types, rhombuses and squares, alias the onsite- and offsite-centered ones [28–30]. First, we consider the pattern-formation dynamics for horizontally kicked rhombic vortices built of four fundamental solitons with an empty site in the center, which carry the total phase circulation of  $2\pi$ , corresponding to the topological charge  $S = 1$ , see Fig. 12(a).



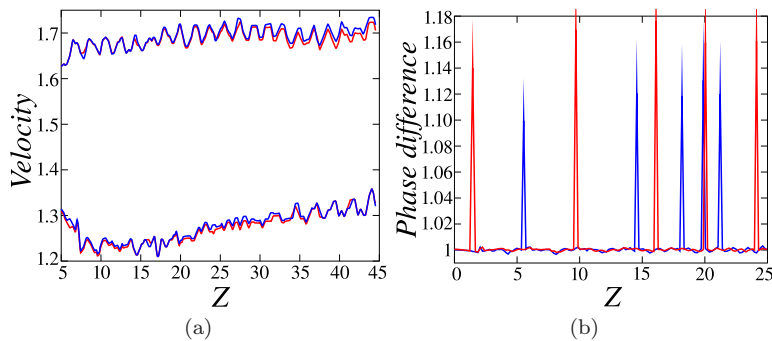


FIG. 11: (Color online) (a) Velocities of two dipoles into which the kicked quadrupole splits at  $k_0 = 3$ . (b) The phase difference inside the two dipoles, in units of  $\pi$ , versus  $Z$ .

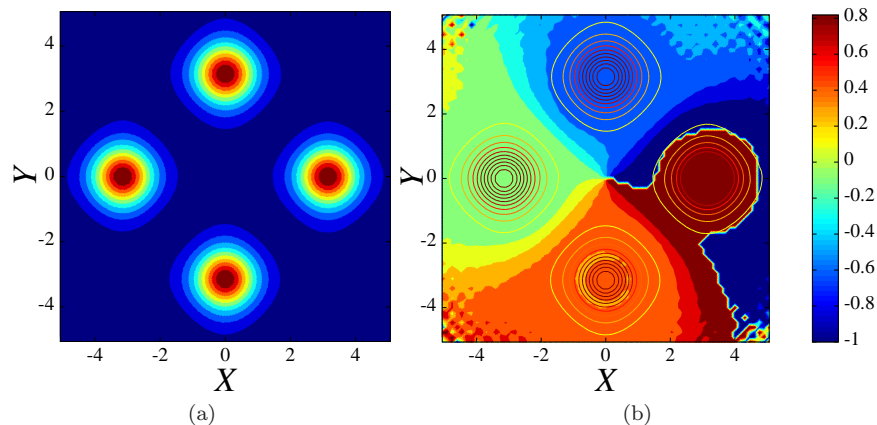


FIG. 12: (Color online) (a) and (b): The distribution of the amplitude and phase (in units of  $\pi$ ) in the stable rhombus-shaped (offsite-centered) vortex.

First, the weak horizontal kick, with  $k_0 \lesssim 0.1$ , excites oscillations of the fundamental solitons, while the vorticity  $S = 1$  is kept (i.e., phase differences between the adjacent solitons remain very close to  $\pi/2$ ), see Fig. 13(b). A stronger kick (for instance,  $k_0 = 0.5$ ) destroys the vortical phase structure, and transforms the vortex into a quadrupole, as shown in Fig. 13(c).

At  $k_0 = 1.0$  and  $k_0 = 1.5$ , see Figs. 14 and 15, respectively, the kick completely destroys the vortices, which are replaced by apparently random clusters of quiescent fundamental solitons. Note that, although the results shown in Figs. 14-15 have not been obtained with periodic b.c. rather than absorbing ones, this circumstance does not affect the results. The same type of b.c. is used below.

### B. Kicked square-shaped (offsite-centered) vortices

Unlike their rhombic counterparts, quiescent square-shaped vortices, such as the one shown in Fig. 16, are unstable in the entire parameter space of Eq. (1) which we have explored, in agreement with the general trend of the offsite-centered vortices to be more fragile than their onsite-centered counterparts [29]. As a result of the instability development, they are transformed into stable quadrupoles. Nevertheless, results displayed below confirm that it is relevant to consider dynamical pattern formation by unstable kicked vortices as this type.

First, we consider the application of the horizontal kick (3) with  $\theta = 0$ , varying its strength  $k_0$ . Similar to the recently studied scenario of the dynamical pattern formation by kicked fundamental solitons [24], the fundamental solitons building the vortex merely oscillate if  $k_0$  takes values below the respective threshold value of  $k_0^{(\text{thr})} = 1.2125$ , cf. Eqs. (5), (6), and (7). It may happen that some of them move towards adjacent sites, in the horizontal direction, and decay later, while the solitons are recovered at the original positions. The inner phase structure of the unstable square-shaped vortex is destroyed in the course of the oscillations, and it transforms into a quadrupole, in accordance with the above-mentioned fact that this is the outcome of its instability in the absence of the kick.

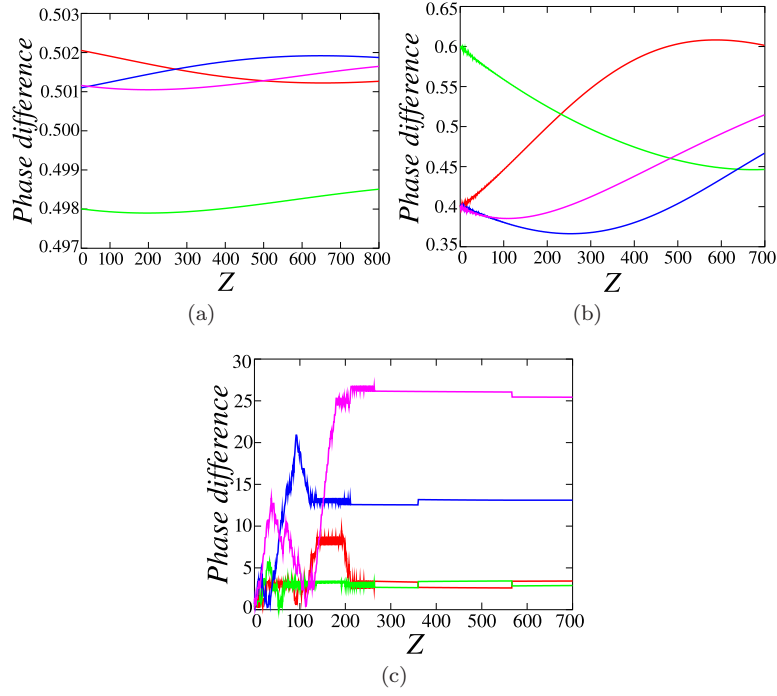


FIG. 13: (Color online) The phase difference between adjacent solitons (in units of  $\pi$ ), versus  $Z$ , in a weakly kicked rhombic vortex, for different values of the kick strength: (a)  $k_0 = 0$ , (b)  $k_0 = 0.1$ , (c)  $k_0 = 0.2$ .

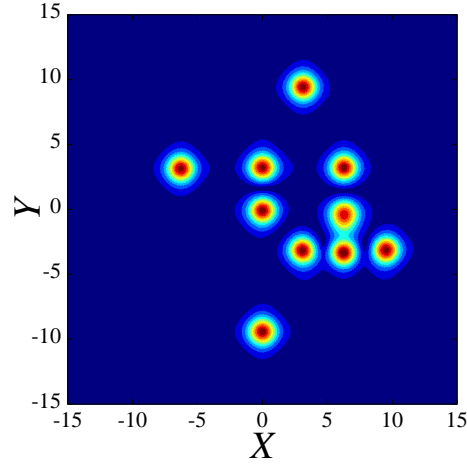


FIG. 14: (Color online) Field  $|u(X, Y)|$  at  $Z = 299.725$ , generated by the kicked rhombic vortex for  $k_0 = 1.0$ .

The increase of  $k_0$  leads to formation of new stable patterns. At  $k_0 = 1.5$ , the right vertical pair (column) of the fundamental solitons, which are a part of the original vortical square, start to duplicate themselves, while moving to the right (in the direction of the kick), see Fig. 17. In fact, the kick breaks the symmetry between the top and bottom solitons in the column, only the bottom one succeeding to create a horizontal array of additional solitons (three ones, in total). In this case, Fig. 18 shows that the eventual value of the total power (2) oscillates between values corresponding to the cumulative power of 7 or 8 quiescent fundamental solitons. The resulting pattern develops seemingly random form, which keeps oscillating, as Figs. 17 (d) and 18 suggest.

At somewhat higher values of  $k_0$  (for example,  $k_0 = 2.0$ ), the original unstable four-soliton set is transformed into a quiescent three-soliton complex, while an extra dipole and a separate free solitons are created and travel through the lattice, see Fig. 19).

With still higher values of  $k_0$ , the number of solitons which remain immobile decreases. Finally, we observe a square-shaped cluster of four solitons moves as a whole, see Figs. 20 and 21, which display the result in both the two-

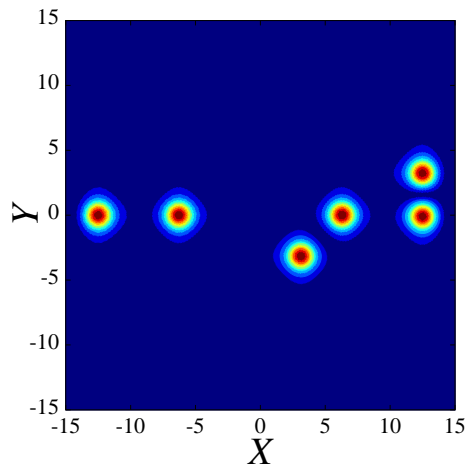


FIG. 15: (Color online) The same as in Fig. 14, but for  $k_0 = 1.5$ .

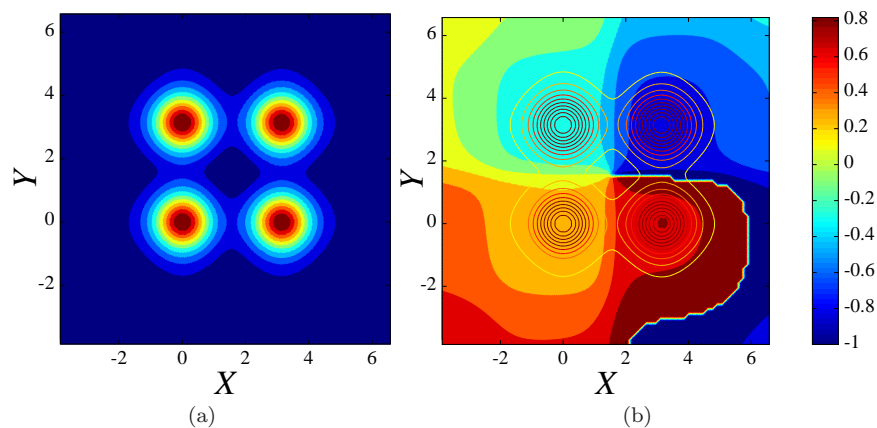


FIG. 16: (Color online) The distribution of the amplitude (a) and phase (b) in the unstable square-shaped (offsite-centered) vortex.

and three-dimensional shapes. However, the cluster does not carry the vortical phase structure.

As shown in Figs. 22 and 23, an intermediate situation occurs too, in which the square-shaped cluster moves as a whole, leaving behind a copy of one of the original solitons. The original square-shaped cluster is absorbed by the right edge.

We have also studied the application of the kick to the square-shaped vortex in other directions, i.e., varying angle  $\theta$  in Eq. (4). First, as seen in Fig. 24(a), in the case of  $\theta = \pi/8$  and  $k_0 = 1.5$ , the kick breaks the symmetry between the top and bottom rows of the solitons, generating an array of additional solitons in the bottom horizontal row. Further, to check that the numerical code is compatible with the global symmetry of the setting, we also considered angles  $\theta = 5\pi/8, 9\pi/8$  and  $13\pi/8$ . The results, shown in Fig. 24, evidence the possibility of controlling the direction of the emission of the soliton array by the direction of the initial kick. In the laser-cavity setup, it corresponds to the direction of the deviation of the incident beam from the axis of the structured medium.

These results can be explained by noting that the intrinsic phase circulation in the vortex is directed counterclockwise (from  $X$  to  $Y$ ). Then, as schematically shown (for example) for  $\theta = \pi/8$  in Fig. 25, the superposition of the externally applied kick (phase gradient) and the intrinsic phase flow gives rise to the largest local phase gradient at the position of the bottom right soliton, in the positive horizontal direction, therefore the array is emitted accordingly.

It is instructive too to perform the simulations for the vortex with the opposite vorticity ( $-1$  instead of  $+1$ ). In this way, the expected symmetry has been verified (not shown here in detail): the same results as above are obtained, with angle  $\theta$  replaced by its counterpart, which is symmetric with respect to the closest coordinate axis.

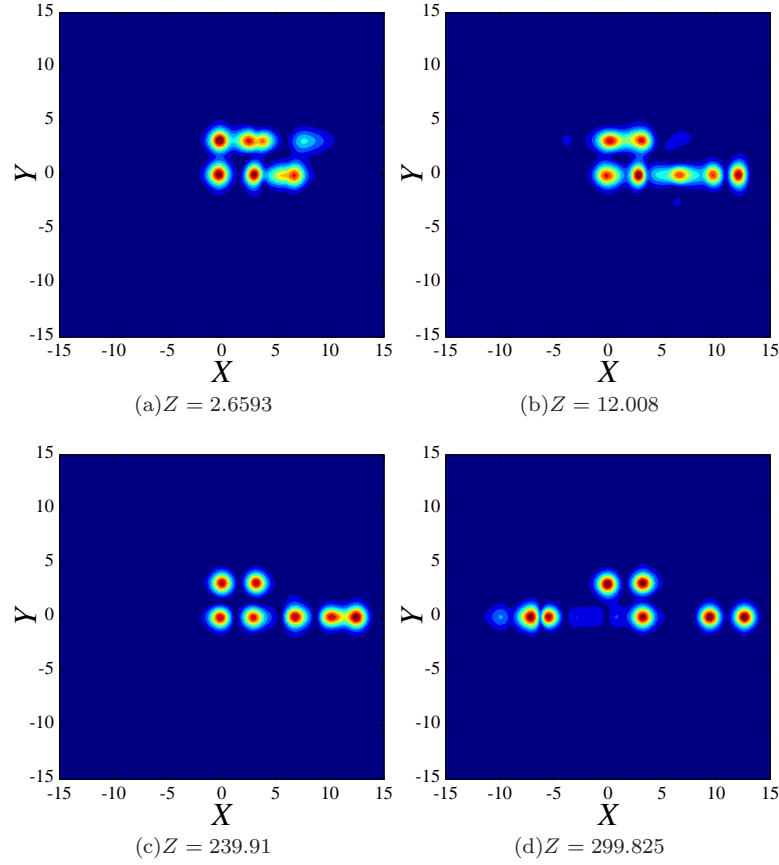


FIG. 17: (Color online) The evolution of the unstable square-shaped (offsite-centered) vortex kicked in the horizontal direction ( $\theta = 0$ ) with  $k_0 = 1.5$ .

## VI. CONCLUSIONS

The objective of this work is to extend the analysis of the dynamical pattern-formation scenarios in the CQ-CGL (cubic-quintic complex Ginzburg-Landau) equation with the 2D cellular potential. The equation models nonlinear laser cavities with a built-in grating, represented by the spatially periodic potential. Recently, the pattern-formation scenarios, initiated by the moving fundamental solitons, were studied in this model. Here, we have systematically analyzed the scenarios produced by kicked compound modes, *viz.*, dipoles, quadrupoles, and vortices of two different types (rhombuses and squares, alias the onsite- and offsite-centered ones). The motion of the kicked compound through the cellular potential leads to the generation of diverse multi-peak patterns pinned to the lattice, which the moving object leaves in its wake. In the annular system with periodic boundary conditions, the persistently traveling dipole hits the pinned pattern from the opposite direction. In this way, several dynamical regimes are initiated, in which the pinned multi-soliton pattern plays the role of the NC (Newton’s cradle), including periodically recurring effective passage of the free dipole through the NC, which suggests realizations of the “cradle” in the form of soliton chains. In fact, this may be the first realization of the NC in dissipative systems. In the case of vortices, the dependence of the outcome of the pattern-formation process on the direction of the kick, with respect to the underlying lattice, was investigated too.

The analysis can be extended by considering two-component systems (which would take the polarization of light into account), collisions between moving modes, and the motion of kicked solitons in inhomogeneous lattices. Eventually, the analysis may be generalized for the three-dimensional setting, which is not relevant to optics, but may be realized, in principle, in terms of Bose-Einstein condensates of polariton-exciton quasiparticles [31].

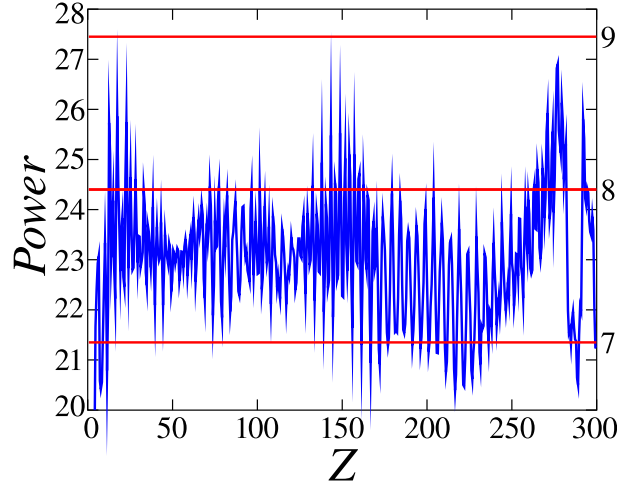


FIG. 18: (Color online) The evolution of the total power for the pattern produced by horizontally kicking the square-shaped vortex, for  $k_0 = 1.5$ . The red horizontal lines show power levels corresponding to  $n$  quiescent solitons.

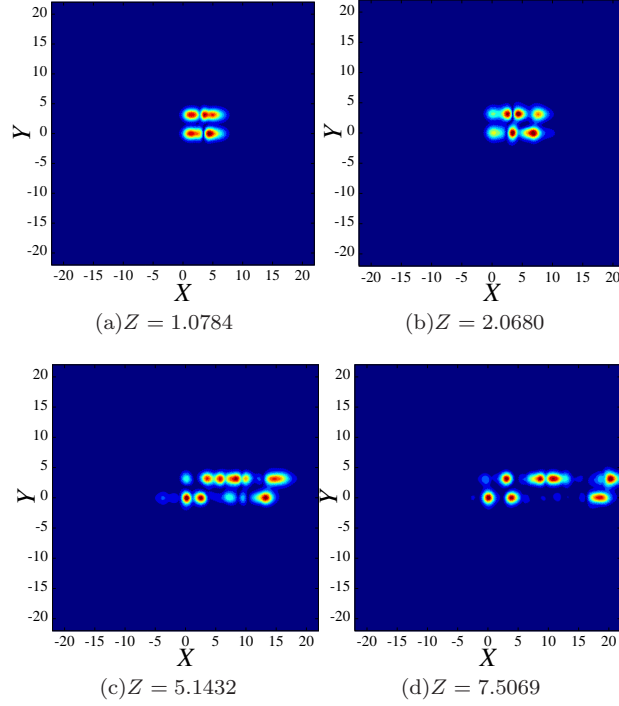


FIG. 19: (Color online) The evolution of the pattern produced by horizontally kicking the square-shaped, for  $k_0 = 2$ .

### Acknowledgements

The work of DM was supported in part by a Senior Chair Grant from the Région Pays de Loire, France. Support from the Romanian Ministry of Education and Research (Project PN-II-ID-PCE-2011-3-0083) is also acknowledged by this author.

---

[1] N. Akhmediev and A. Ankiewicz (Eds.), *Dissipative Solitons*, Lect. Notes Phys. **661**, Springer, Berlin, 2005; N. Akhmediev and A. Ankiewicz (Eds.), *Dissipative Solitons: From Optics to Biology and Medicine*, Lect. Notes Phys. **751**, Springer,

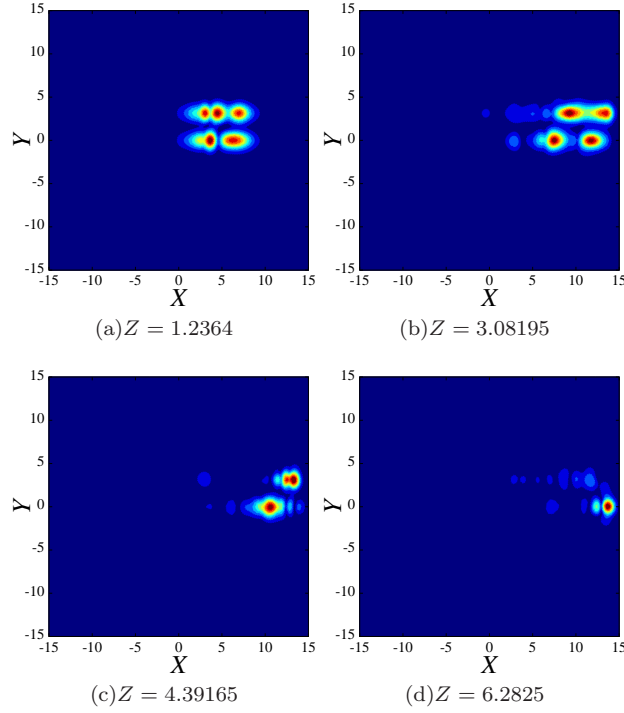


FIG. 20: (Color online) The pattern produced by the horizontally kicked square-shaped vortex, at  $k_0 = 3.0$ .

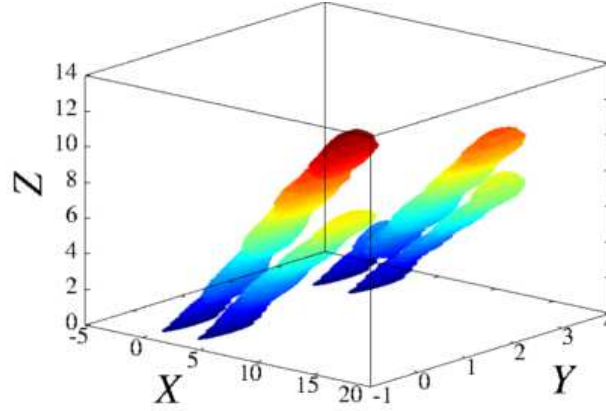


FIG. 21: (Color online) The three-dimensional rendition of the evolution of the original horizontally kicked square-shaped vortex for  $k_0 = 3.0$ . The chromatic progression indicates the propagation direction.

Berlin, 2008.

- [2] N. N. Rosanov, *Spatial Hysteresis and Optical Patterns* (Springer, Berlin, 2002).
- [3] S. Barland, J. R. Tredicce, M. Brambilla, L. A. Lugiato, S. Balle, M. Giudici, T. Maggipinto, L. Spinelli, G. Tissoni, T. Knödl, M. Miller, and R. Jäger, *Nature (London)* **419**, 699 (2002); Z. Bakonyi, D. Michaelis, U. Peschel, G. Onishchukov, and F. Lederer, *J. Opt. Soc. Am. B* **19**, 487 (2002); E. A. Ultanir, G. I. Stegeman, D. Michaelis, C. H. Lange, and F. Lederer, *Phys. Rev. Lett.* **90**, 253903 (2003); P. Mandel and M. Tlidi, *J. Opt. B: Quantum Semiclass. Opt.* **6**, R60 (2004); N. N. Rosanov, S. V. Fedorov, and A. N. Shatsev, *Appl. Phys. B* **81**, 937 (2005); C. O. Weiss and Ye. Larionova, *Rep. Progr. Phys.* **70**, 255 (2007); N. Veretenov and M. Tlidi, *Phys. Rev. A* **80**, 023822 (2009); M. Tlidi, A. G. Vladimirov, D. Pieroux, and D. Turaev, *Phys. Rev. Lett.* **103**, 103904 (2009); P. Genevet, S. Barland, M. Giudici, and J. R. Tredicce, *Phys. Rev. Lett.* **104**, 223902 (2010); P. Grelu and N. Akhmediev, *Nature Photonics*, **6**, 84 (2012); J. Jiménez, Y. Noblet, P. V. Paulau, D. Gomila, and T. Ackemann, *J. Opt.* **15**, 044011 (2013); C. Fernandez-Oto, M. G. Clerc, D. Escaff, and M. Tlidi, *Phys. Rev. Lett.* **110**, 174101 (2013).
- [4] N. Lazarides and G. P. Tsironis, *Phys. Rev. E* **71**, 036614 (2005); Y. M. Liu, G. Bartal, D. A. Genov, and X. Zhang, *Phys. Rev. Lett.* **99**, 153901 (2007); E. Feigenbaum and M. Orenstein, *Opt. Lett.* **32**, 674 (2007); I. R. Gabitov, A. O. Korotkevich, A. I. Maimistov, and J. B. Mcmahon, *Appl. Phys. A* **89**, 277 (2007); A. R. Davoyan, I. V. Shadrivov, and Y.



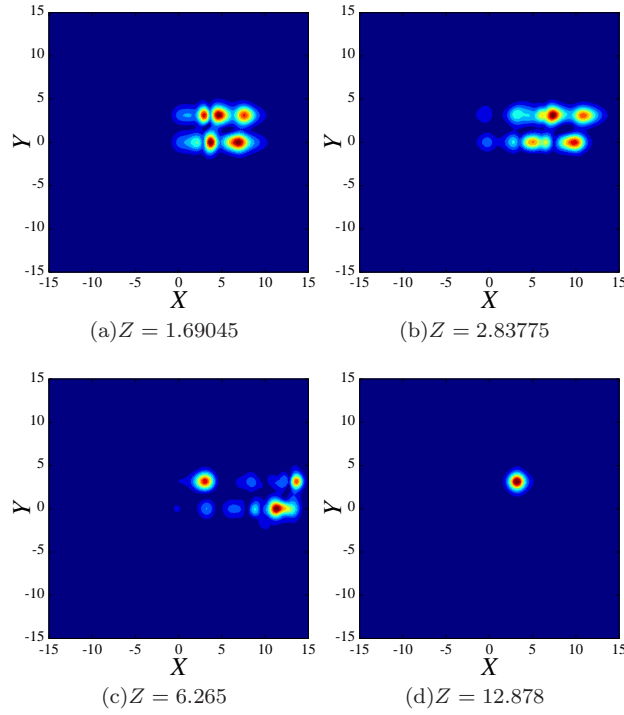


FIG. 22: (Color online) The same as in Fig. 20, but for  $k_0 = 2.5$ .

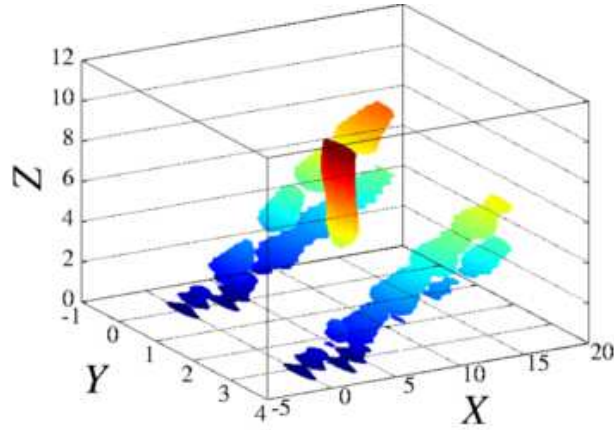


FIG. 23: (Color online) The same as in Fig. 20 for  $k_0 = 2.5$ . In particular, the vertical rod represents the additional quiescent fundamental soliton, left in the wake of the moving four-soliton cluster.

- S. Kivshar, *Opt. Exp.* **17**, 21732 (2009); K. Y. Bliokh, Y. P. Bliokh, and A. Ferrando, *Phys. Rev. A* **79**, 041803 (2009); E. V. Kazantseva and A. I. Maimistov, *ibid.* **79**, 033812 (2009); Y.-Y. Lin, R.-K. Lee, and Y. S. Kivshar, *Opt. Lett.* **34**, 2982 (2009); A. Marini and D. V. Skryabin, *ibid.* **81**, 033850 (2010); A. Marini, D. V. Skryabin, and B. A. Malomed, *Opt. Exp.* **19**, 6616 (2011).
- [5] V. I. Petviashvili and A. M. Sergeev, *Dokl. AN SSSR* **276**, 1380 (1984) [*Sov. Phys. Doklady* **29**, 493 (1984)].
- [6] I. S. Aranson and L. Kramer, *Rev. Mod. Phys.* **74**, 99 (2002); B. A. Malomed, in *Encyclopedia of Nonlinear Science*, p. 157. A. Scott (Ed.), Routledge, New York, 2005.
- [7] J. Anglin, *Phys. Rev. Lett.* **79**, 6 (1997); F. T. Arecchi, J. Bragard, and L. M. Castellano, *Opt. Commun.* **179**, 149 (2000); J. Keeling and N. G. Berloff, *Phys. Rev. Lett.* **100**, 250401 (2008); B. A. Malomed, O. Dzyapko, V. E. Demidov, and S. O. Demokritov, *Phys. Rev. B* **81**, 024418 (2010); H. Deng, H. Haug, and Y. Yamamoto, *Rev. Mod. Phys.* **82**, 1489 (2010); B. Deveaud-Plédran, *J. Opt. Soc. Am. B* **29**, A138 (2012).
- [8] M. C. Cross and P. C. Hohenberg, *Rev. Mod. Phys.* **65**, 851 (1993).
- [9] K.-H. Hoffmann and Q. Tang, *Ginzburg-Landau Phase Transition Theory and Superconductivity* (Birkhauser Verlag: Basel, 2001).

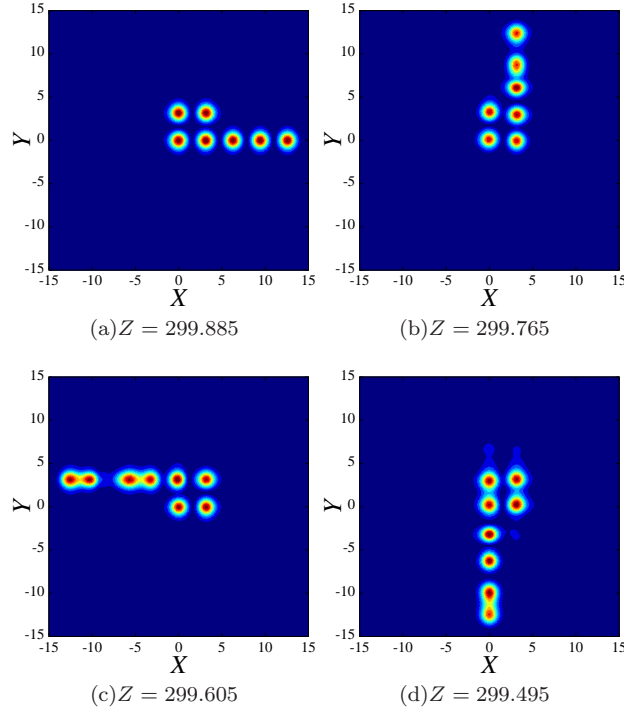


FIG. 24: (Color online) The pattern produced by the square-shaped vortex kicked with strength  $k_0 = 1.5$  in different directions: (a)  $\theta = \pi/8$ ; (b)  $\theta = 5\pi/8$ ; (c)  $\theta = 9\pi/8$ ; (d)  $\theta = 13\pi/8$ .

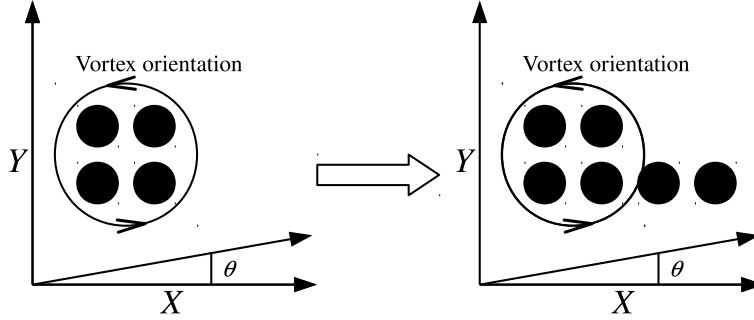


FIG. 25: The explanation of the direction in which the soliton array is emitted from the kicked square-shaped vortex.

- [10] B. A. Malomed, *Physica D* **29**, 155 (1987).
- [11] O. Thual and S. Fauve, *J. Phys. (Paris)* **49**, 1829 (1988); S. Fauve and O. Thual, *Phys. Rev. Lett.* **64**, 282 (1990); W. van Saarloos and P. C. Hohenberg, *Phys. Rev. Lett.* **64**, 749 (1990); V. Hakim, P. Jakobsen, and Y. Pomeau, *Europhys. Lett.* **11**, 19 (1990); B. A. Malomed and A. A. Nepomnyashchy, *Phys. Rev. A* **42**, 6009 (1990); P. Marcq, H. Chaté, R. Conte, *Physica D* **73**, 305 (1994); N. Akhmediev and V. V. Afanasjev, *Phys. Rev. Lett.* **75**, 2320 (1995); H. R. Brand and R. J. Deissler, *Phys. Rev. Lett.* **63**, 2801 (1989); V. V. Afanasjev, N. Akhmediev, and J. M. Soto-Crespo, *Phys. Rev. E* **53**, 1931 (1996); J. M. Soto-Crespo, N. Akhmediev, and A. Ankiewicz, *Phys. Rev. Lett.* **85**, 2937 (2000); H. Leblond, A. Komarov, M. Salhi, A. Haboucha, and F. Sanchez, *J. Opt. A: Pure Appl. Opt.* **8**, 319 (2006); W. H. Renninger, A. Chong, and F. W. Wise, *Phys. Rev. A* **77**, 023814 (2008); J. M. Soto-Crespo, N. Akhmediev, C. Mejia-Cortes, and N. Devine, *Opt. Express* **17**, 4236 (2009); D. Mihalache, *Proc. Romanian Acad. A* **11**, 142 (2010); Y. J. He, B. A. Malomed, D. Mihalache, F. W. Ye, and B. B. Hu, *J. Opt. Soc. Am. B* **27**, 1266 (2010); D. Mihalache, *Rom. Rep. Phys.* **63**, 325 (2011); C. Mejia-Cortes, J. M. Soto-Crespo, R. A. Vicencio, and M. I. Molina, *Phys. Rev. A* **83**, 043837 (2011); D. Mihalache, *Rom. J. Phys.* **57**, 352 (2012); O. V. Borovkova, V. E. Lobanov, Y. V. Kartashov, and L. Torner, *Phys. Rev. A* **85**, 023814 (2012).
- [12] L.-C. Crasovan, B. A. Malomed, and D. Mihalache, *Phys. Rev. E* **63**, 016605 (2001); *Phys. Lett. A* **289**, 59 (2001); D. Mihalache, D. Mazilu, F. Lederer, Y. V. Kartashov, L.-C. Crasovan, L. Torner, and B. A. Malomed, *Phys. Rev. Lett.* **97**, 073904 (2006); D. Mihalache, D. Mazilu, F. Lederer, H. Leblond, and B. A. Malomed, *Phys. Rev. A* **76**, 045803 (2007);

- ibid.* **75**, 033811 (2007); D. Mihalache and D. Mazilu, Rom. Rep. Phys. **60**, 749 (2008).
- [13] M. Tlidi, M. Haelterman, and P. Mandel, Europhys. Lett. **42**, 505 (1998); M. Tlidi and P. Mandel, Phys. Rev. Lett. **83**, 4995 (1999); M. Tlidi, J. Opt. B: Quantum Semiclass. Opt. **2**, 438 (2000).
- [14] H. Sakaguchi, Physica D **210**, 138 (2005).
- [15] V. Skarka and N. B. Aleksić, Phys. Rev. Lett. **96**, 013903 (2006); N. B. Aleksić, V. Skarka, D. V. Timotijević, and D. Gauthier, Phys. Rev. A **75**, 061802 (2007); V. Skarka, D. V. Timotijević, and N. B. Aleksić, J. Opt. A: Pure Appl. Opt. **10**, 075102 (2008); V. Skarka, N. B. Aleksić, H. Leblond, B. A. Malomed, and D. Mihalache, Phys. Rev. Lett. **105**, 213901 (2010).
- [16] A. Szameit, J. Burghoff, T. Pertsch, S. Nolte, and A. Tünnermann, Opt. Exp. **14**, 6055 (2006).
- [17] J. W. Fleischer, M. Segev, N. K. Efremidis, and D. N. Christodoulides, Nature **422**, 147 (2003).
- [18] H. Leblond, B. A. Malomed, and D. Mihalache, Phys. Rev. A **80**, 033835 (2009).
- [19] W. J. Firth and A. Scroggie, Phys. Rev. Lett. **76**, 1623 (1996).
- [20] M. Brambilla, A. Gatti and L. A. Lugiato, Adv. At. Molec. Opt. Phys. **40**, 229 (1998).
- [21] S. V. Fedorov, A. G. Vladimirov, G. V. Khodova, N. N. Rosanov, Phys. Rev. E **61**, 5814 (2000).
- [22] D. Mihalache, D. Mazilu, V. Skarka, B. A. Malomed, H. Leblond, N. B. Aleksić, and F. Lederer, Phys. Rev. A **82**, 023813 (2010).
- [23] D. Mihalache, D. Mazilu, F. Lederer, H. Leblond, and B. A. Malomed, Phys. Rev. A **81**, 025801 (2010).
- [24] V. Besse, H. Leblond, D. Mihalache, and B. A. Malomed, Phys. Rev. E **87**, 012916 (2013).
- [25] A. V. Ustinov, Phys. Lett. A **136**, 155 (1989); B. A. Malomed, Phys. Rev. B **41**, 26166 (1990); A. Shnirman, Z. Hermon, A. V. Ustinov, B. A. Malomed, and E. Ben-Jacob, *ibid.* B **50**, 12793 (1994).
- [26] D. Novoa, B. A. Malomed, H. Michinel, and V. M. Pérez-García, Phys. Rev. Lett. **101**, 144101 (2008).
- [27] R. Driben, B. A. Malomed, A. V. Yulin, and D. V. Skryabin, Phys. Rev. A **87**, 063808 (2013).
- [28] B. B. Baizakov, B. A. Malomed, and M. Salerno, Europhys. Lett. **63**, 642 (2003); J. Yang and Z. H. Musslimani, Opt. Lett. **28**, 2094 (2003).
- [29] T. Mayteevarunyoo, B. A. Malomed, B. B. Baizakov, and M. Salerno, Physica D **238**, 1439 (2009).
- [30] J. Yang, *Nonlinear Waves in Integrable and Nonintegrable Systems* (SIAM: Philadelphia, 2010).
- [31] H. Deng, H. Haug, and Y. Yamamoto, Rev. Mod. Phys. **82**, 1489 (2010); B. Deveaud-Plédran, J. Opt. Soc. Am. B **29**, A138 (2012); N. G. Berloff and J. Keeling, arXiv:1303.6195v2.